



PERGAMON

Mechanism and Machine Theory 37 (2002) 895–913

**MECHANISM
AND
MACHINE THEORY**

www.elsevier.com/locate/mechmt

A comparison of revolute joint clearance models in the dynamic analysis of rigid and elastic mechanical systems

A.L. Schwab ^{*}, J.P. Meijaard, P. Meijers

Laboratory for Engineering Mechanics, Delft University of Technology, Mekelweg 2, NL-2628 CD Delft, Netherlands

Received 11 January 2001; accepted 28 January 2002

Abstract

The dynamic response of mechanisms and machines affected by revolute joint clearance is studied in this article. Critical in the precise prediction of the peak values of forces is the contact model being used. A comparison is made between several continuous contact force models and an impact model. The mechanical system is modelled with rigid or elastic bodies. For the impact model a procedure is presented to estimate the maximum contact force during impact. It is shown how the compliance of the links or lubrication of the joint smooths the peak values of the contact forces.

© 2002 Elsevier Science Ltd. All rights reserved.

Résumé

La réponse dynamique des mécanismes et des machines en présence de jeu dans les pivots est étudiée dans cet article. La modélisation du contact est un aspect critique pour une prédiction précise des valeurs extrêmes des forces. Plusieurs modèles avec force de contact continue ainsi qu'un modèle d'impact sont comparés. Le système mécanique est modélisé par des corps rigides et flexibles. Pour le modèle d'impact, une procédure d'estimation de la force de contact maximum durant l'impact est présentée. Nous montrons comment la flexibilité des membres du mécanisme et la lubrification des joints réduisent les valeurs extrêmes des forces de contact.

© 2002 Elsevier Science Ltd. All rights reserved.

1. Introduction

Joint clearances due to manufacturing tolerances and wear can seriously affect the dynamic response of mechanical systems. In unlubricated joints it is usually accompanied by rattling,

^{*} Corresponding author. Fax: +31-15-278-2150.

E-mail address: a.l.schwab@wbmt.tudelft.nl (A.L. Schwab).

excessive wear and noise, which is caused by peak contact forces. A critical factor in the prediction of the peak forces is the contact model being used. In the past a considerable amount of experimental and theoretical work has been done to study the effect of joint clearances on the dynamic response of mechanical systems. An overview of the English language literature on this subject up to 1980 is given by Haines [1]. In an early German study Hain [2] discusses the effect of radial joint clearance on the forces in an experimental set-up of a scotch-yoke mechanism. After 1980 Soong and Thompson [3] did experimental work on a slider-crank mechanism with revolute joint clearance between the connecting rod and the slider and they made a comparison with calculated results from a rigid-link model. A spatial manipulator with joint clearance was modelled by Kakizaki et al. [4], who included the effects of elastic links and the control system. Deck and Dubowsky [5] published experimental results on a spatial slider-crank mechanism. The possibility of occurrence of chaotic motion was shown by Seneviratne and Earles [6].

This article will focus on the modelling of joint clearances in a computer code environment for dynamic analysis of mechanical systems. First of all the kinematics of a planar journal bearing will be discussed. In the subsequent section two continuous contact force models are treated, a Hertzian contact model with dissipation and a lubricated, hydrodynamic bearing model. Both models are applied in illustrative examples. In Section 4 the basic equations for a discontinuous contact force model (impact with rebound) in a mechanical system are derived. The numerical aspects of such an analysis are treated in depth and an estimate for the maximum contact force during impact is presented. The various contact models are illustrated for a high-speed slider-crank mechanism with a revolute joint clearance between the connecting rod and the slider. The results for the case of rigid links and Hertzian contact forces obtained with a finite element based multibody software system are compared with results as presented by Ravn [7].

2. Joint clearance model

Joint clearance in a planar revolute joint (see Fig. 1) is usually modelled by the introduction of two extra degrees of freedom, the horizontal and the vertical displacements, x and y , of the journal centre relative to the sleeve centre. Since the relative rotation is unconstrained this means

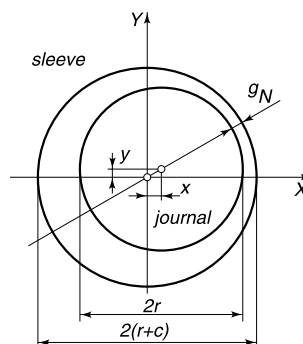


Fig. 1. Planar revolute joint with clearance.

that in a non-contact condition no constraints are introduced by the joint. The interaction between the two parts in the joint is solely achieved by normal and tangential contact forces.

The kinematic contact condition for a revolute joint with radial clearance c and relative displacements x and y is given by

$$g_N = c - \sqrt{x^2 + y^2} \leq 0. \quad (1)$$

No contact corresponds to $g_N > 0$ while contact with local deformation near the contact zone, to be indicated as penetration, is denoted by a negative value of g_N . When the journal comes into contact with the sleeve and the contact is assumed rigid, one degree of freedom vanishes. The two remaining degrees of freedom are a relative rotation of the two parts and a rotation of the journal centre around the sleeve centre. In the case of friction in the contact region there is a possibility of sticking. When sticking occurs, again a degree of freedom disappears and there is only one possible relative motion in which the cylindrical surface of the journal rolls without slip along the inner sleeve surface.

3. Continuous contact force models

3.1. Hertzian contact force model with dissipation

Since we are not interested in the shape nor any other detail of the contact region, we need only a global contact model with few parameters. For an unlubricated joint the Hertzian contact force model is an appropriate choice. Whereas the original Hertzian model does not include any energy dissipation, an extension by Lankarani and Nikravesh [8,9] includes energy loss due to internal damping. In this model the compressive contact force F_N in terms of the penetration depth $\delta = -g_N$, and velocity $\dot{\delta} = -\dot{g}_N$, is given by

$$F_N = \begin{cases} K\delta^n + D\dot{\delta} & \delta > 0 \\ 0 & \delta \leq 0. \end{cases} \quad (2)$$

For the frictionless Hertzian contact between two spheres [10] the exponent $n = 3/2$ and the stiffness parameter K is given by

$$K = \frac{4}{3\pi(h_1 + h_2)} \sqrt{\bar{R}}, \quad (3)$$

where

$$\bar{R} = \frac{R_1 R_2}{R_1 + R_2}; \quad h_i = \frac{1 - \nu_i^2}{\pi E_i} \quad i = 1, 2$$

with radius R_i , Poisson's ratio ν_i and Young's modulus E_i associated with each sphere. A form for the hysteretic damping coefficient according to

$$D = H\delta^n, \quad (4)$$

was proposed by Hunt and Crossley [11]. The so-called hysteretic damping factor H can be estimated from a comparison of the energy loss at a central impact of two spheres with coefficient of restitution e and the energy loss after one hysteretic loop, yielding

$$H = \frac{3K(1 - e^2)}{4\dot{\delta}^-}, \quad (5)$$

with $\dot{\delta}^-$ the penetration velocity just before impact. A major drawback of this model is the dependency of the hysteretic damping factor H on the impact velocity $\dot{\delta}^-$. In finding this we have to track down the precise moment of impact which makes the continuous model partly non-smooth. Furthermore it can be shown that the approximate model underestimates the amount of dissipated energy, and consequently results in a higher velocity after impact. For a restitution factor e of 0.75 and above, the error in the velocity after impact is less than 10%, while the error in the dissipated energy is less than 25%. This contact law is derived for colliding spheres having circular contact regions. In the case of a planar revolute joint we have to deal with cylindrical line contact. This line contact will only be present when we have two extremely precise aligned long cylinders. This is usually not the case and therefore Harris [12] proposes that the sphere contact model should be used. According to Ravn [7] this is reasonably close to the more complicated force–displacement relation for cylindrical line contact.

An illustrative example of the dissipative Hertzian contact force model is an elastic sphere impacting an elastic barrier. The parameters for this example are chosen in conformity with those of the slider-crank example to be discussed in Section 5. The sphere with radius $R_i = 9.5$ mm and mass $m = 0.145$ kg has an initial velocity just before impact of $\dot{\delta}^- = 5$ m/s. The fixed barrier has a concave spherical curvature with radius $R_j = -10.0$ mm. The materials in contact have the properties of steel with Young's modulus $E = 2.06 \times 10^{11}$ N/m², Poisson's ratio $\nu = 0.3$ and coefficient of restitution $e = 0.95$. Fig. 2 shows the penetration depth, the contact force and the hysteretic loop for a typical impact.

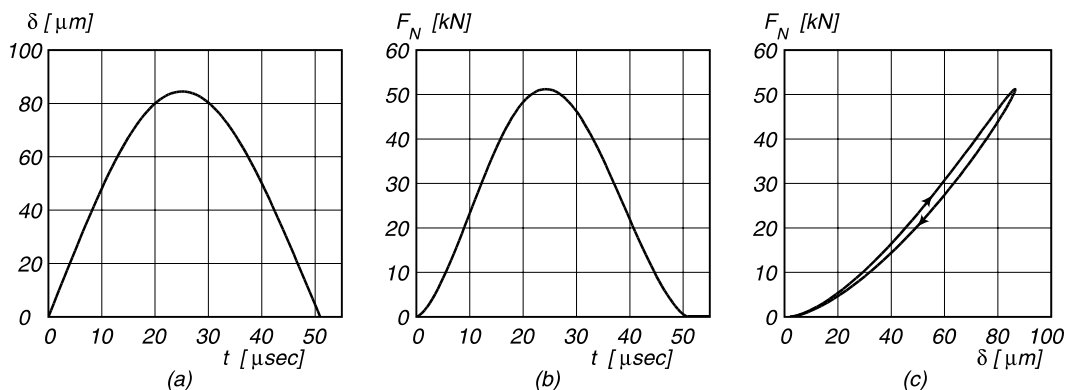


Fig. 2. Hertzian contact law according to (2) with penetration depth δ , contact force F_N and hysteretic loop of a sphere impacting a barrier; $m = 0.145$ kg; $\dot{\delta}^- = 5$ m/s; $K = 65.8 \times 10^9$ N/m^{1.5}; $e = 0.95$.

3.2. Hydrodynamic contact force model

Since most of the joint clearances in mechanisms and machines are in lubricated bearings, a model is needed for this type of bearing. The simplest type of fluid film bearing for a revolute joint is the plane full journal bearing. Rogers and Andrews [13] are among the few who incorporate a simple empirical hydrodynamic bearing model in a linkage dynamic analysis. In the work of Moes et al. [14] simple but nevertheless accurate closed-form analytical expressions for the load carrying properties of fluid film bearings are introduced. These solutions are based upon the Reynolds equation for a thin film. Incorporated is the effect of cavitation and the finite length of the bearing. An algorithmic interpretation of their expressions for the determination of the bearing force as a function of the relative position and speed of the journal and the physical parameters of the bearing is presented in Appendix A. This straightforward algorithm can be coded in any numerical procedure. It returns the forces exerted by the fluid film on the sleeve expressed in the Cartesian reference frame Oxy of the sleeve as

$$\begin{bmatrix} F_x \\ F_y \end{bmatrix} = 2\mu l \left(\frac{r}{c}\right)^3 v_s \begin{bmatrix} \cos \varphi & -\sin \varphi \\ \sin \varphi & \cos \varphi \end{bmatrix} \begin{bmatrix} W_x \\ W_y \end{bmatrix}, \tag{6}$$

with journal radius r , radial clearance c , bearing length l , lubricant dynamic viscosity μ , pure-squeeze velocity magnitude v_s and orientation φ , and dimensionless damping coefficients W_x and W_y which are a function of the shape and the state of motion of the bearing. An example of the quasi-static load carrying capacity of such a lubricated journal bearing is shown in Fig. 3. The sleeve is fixed and the journal rotates with a constant angular velocity. The bearing force with respect to the fixed frame is calculated as a function of the scaled horizontal position x/c . In every position the velocities \dot{x} and \dot{y} are zero (quasi-static). The bearing dimensions are the same as those of the slider-crank example from Section 5. From this example a major characteristic of the bearing model is immediately clear: when the journal approaches the sleeve, e.g. $x/c > 0.95$, the bearing force increases very rapidly; note the logarithmic scale used. The bearing becomes stiff and the numerical analysis will be sensitive to small errors in the relative journal positions x and y .

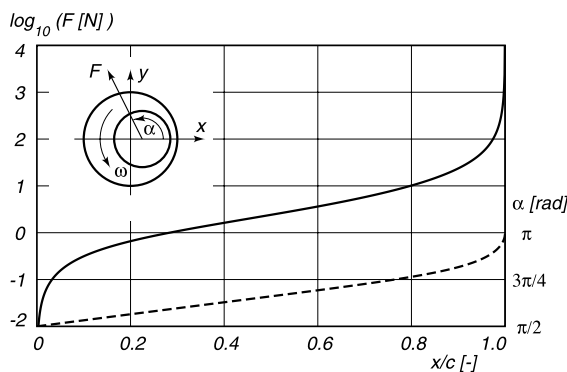


Fig. 3. Bearing force F in magnitude (—) and orientation (---) exerted by the lubricant on the journal as a function of the eccentricity $x/c(y = 0)$ for the quasi-static case ($\dot{x} = 0$ and $\dot{y} = 0$), with a hydrodynamic lubricated bearing according to the model by Moes et al. [14]; $\omega = 163.62$ rad/s; $r = 10.0$ mm; $c = 0.5$ mm; $l = 2r$; $\mu = 0.1$ N s/m².

4. Discontinuous contact force model

4.1. Impulse equations

In the discontinuous contact force model the duration of contact is assumed to be very short in comparison with the time scale of the problem at hand. Under this assumption the change in velocity is instantaneous and we speak of an impact. The velocity jump is enforced by a very high value of the contact force acting only during a small time interval of contact. In the limit case the force is infinite and the time interval is zero. The integral of the force with respect to time over the duration of the impact, the impulse, has a finite value which is the cause of the velocity jump. While the impact takes place all positions remain constant and all non-impulsive forces of the mechanical system can be neglected. The impact is usually divided into a compression and an expansion phase. Newton's impact law links these two phases by stating that the relative speed after impact equals e times the relative speed before impact but it has the opposite direction. The factor e is the coefficient of restitution. A value of $e = 1$ corresponds with a fully elastic impact whereas the value of $e = 0$ represents a completely inelastic impact in which the two parts "stick" together after impact. For an unconstrained mechanical system the equations of motion can be written as

$$\mathbf{M}\ddot{\mathbf{q}} = \mathbf{f}, \quad (7)$$

with mass matrix \mathbf{M} , the accelerations $\ddot{\mathbf{q}}$ of the generalized coordinates \mathbf{q} and the sum of all generalized forces \mathbf{f} . When contact occurs possibly at a number of points, indicated by the vector equation $\mathbf{g}_N(\mathbf{q}) = \mathbf{0}$, the system becomes constrained and the equations of motion become

$$\mathbf{M}\ddot{\mathbf{q}} + \mathbf{g}_N^T \lambda_N = \mathbf{f}, \quad (8)$$

with the partial derivatives $\mathbf{g}'_N = \partial \mathbf{g}_N / \partial \mathbf{q}$ and the multipliers λ_N dual to the relative contact velocities $\dot{\mathbf{g}}_N$. These multipliers can be interpreted as the contact forces. Integration of these equations of motion over the time of impact and taking the limit case yields

$$\lim_{t^- \uparrow t^+} \int_{t^-}^{t^+} (\mathbf{M}\ddot{\mathbf{q}} + \mathbf{g}_N^T \lambda_N) dt = \mathbf{0}. \quad (9)$$

The generalized forces \mathbf{f} only contain non-impulsive forces and therefore the right-hand side vanishes. Under the introduction of the contact impulses,

$$\mathbf{s}_N = \lim_{t^- \uparrow t^+} \int_{t^-}^{t^+} \lambda_N dt, \quad (10)$$

and noting that the mass matrix, in general a function of the generalized coordinates, stays constant during impact, the momentum equations for the mechanical system become

$$\mathbf{M}\dot{\mathbf{q}}^+ + \mathbf{g}_N^T \mathbf{s}_N = \mathbf{M}\dot{\mathbf{q}}^-, \quad (11)$$

with $\dot{\mathbf{q}}^-$ the generalized velocities before and $\dot{\mathbf{q}}^+$ the generalized velocities after impact. Together with Newton's impact law,

$$\dot{\mathbf{g}}_N^+ = -e\dot{\mathbf{g}}_N^-, \quad \text{or} \quad \mathbf{g}'_N \dot{\mathbf{q}}^+ = -e\mathbf{g}'_N \dot{\mathbf{q}}^-, \quad (12)$$

we have a complete set of linear equations reading

$$\begin{bmatrix} \mathbf{M} & \mathbf{g}'_N{}^T \\ \mathbf{g}'_N & \mathbf{0} \end{bmatrix} \begin{bmatrix} \dot{\mathbf{q}}^+ \\ \mathbf{s}_N \end{bmatrix} = \begin{bmatrix} \mathbf{M}\dot{\mathbf{q}}^- \\ -e\mathbf{g}'_N \dot{\mathbf{q}}^- \end{bmatrix}. \quad (13)$$

From these equations the velocities after impact $\dot{\mathbf{q}}^+$ together with the contact impulses \mathbf{s}_N can be found. Because Newton's impact law (12) is often contradicted experimentally in case of multiple impacts, a restriction to simple impacts is made. With one impact occurring at a time the resulting contact impulse can be solved as

$$\mathbf{s}_N = (1 + e)m_e \mathbf{g}'_N \dot{\mathbf{q}}^-, \quad (14)$$

where the effective mass

$$m_e = 1/(\mathbf{g}'_N \mathbf{M}^{-1} \mathbf{g}'_N{}^T). \quad (15)$$

The velocities after impact are given by

$$\dot{\mathbf{q}}^+ = \dot{\mathbf{q}}^- - \mathbf{M}^{-1} \mathbf{g}'_N{}^T \mathbf{s}_N. \quad (16)$$

The change of energy during impact is equal to the difference of the kinetic energy before and after the impact yielding

$$\Delta T = -\frac{1}{2}(1 - e^2)m_e(\dot{\mathbf{g}}_N^-)^2. \quad (17)$$

Since the coefficient of restitution e is between 0 and 1, the impact will always be dissipative except for the limit case $e = 1$, where we have energy conservation.

4.2. Numerical aspects of impact analysis

In a joint having a clearance three distinct states are to be observed: free flight where there is no contact between the two parts, impact and permanent contact. In doing the numerical calculations it is very important to find the precise moment in time of transition between these different states. If not, there will be a build-up of errors and the final results are inaccurate. If we rely on the integration routine to do this job it has to step back and take smaller steps until a step is taken within the error tolerance. The transition from an impacting motion to permanent contact leads to an infinite number of impacts (with decreasing impact velocities) in a finite period of time, a so-called finite time singularity. In the next three subsections the handling of the different transitions will be treated.

4.2.1. Contact detection

Usually coming into contact is detected by a change of sign in the distance g_N between the discrete moments in time t_n and t_{n+1} ,

$$g_N(\mathbf{q}(t_n))g_N(\mathbf{q}(t_{n+1})) < 0. \quad (18)$$

This zero crossing of $g_N(\mathbf{q}(t))$ can be found with the help of a bisection or a Newton–Raphson procedure. In both cases we need to calculate intermediate values of $\mathbf{q}(t)$. A fast and accurate

approach, as proposed by Meijaard [15], uses a third-order interpolation polynomial between the already calculated position and velocity at t_n and t_{n+1} . This interpolation reads

$$\mathbf{q}(t) = (1 - 3\xi^2 + 2\xi^3)\mathbf{q}(t_n) + (\xi - 2\xi^2 + \xi^3)h\dot{\mathbf{q}}(t_n) + (3\xi^2 - 2\xi^3)\mathbf{q}(t_{n+1}) + (-\xi^2 + \xi^3)h\dot{\mathbf{q}}(t_{n+1}) \quad (19)$$

with $\xi = (t - t_n)/h$ and $h = t_{n+1} - t_n$. By interpolation of the generalized coordinates $\mathbf{q}(t)$ and evaluation of the distance function $g_N(\mathbf{q}(t))$ the moment of contact can be calculated within a given error tolerance. We thus avoid repetitive calculation of the accelerations from the system equations to find the zero crossing.

4.2.2. Permanent contact

Just as with a bouncing ball on a horizontal plane, the journal may tend to stay in permanent contact with the sleeve. In the analysis this is often recognized as a rapidly increasing number of impacts with decreasing impulses. On the basis of slowly varying forces the motion, after impact with such a low impact velocity, can be estimated by a constant acceleration flight,

$$g_N(t_n + h) = \dot{g}_N(t_n)h + \frac{1}{2}\ddot{g}_N(t_n)h^2. \quad (20)$$

The next moment of contact is estimated by setting $g_N(t_n + h)$ to zero from which we come up with an estimated duration between contacts,

$$h_c = -2\frac{\dot{g}_N}{\ddot{g}_N}. \quad (21)$$

If this estimated duration is within the integration timestep, contact within one integration step is highly probable. The time in which permanent contact will occur can be estimated by assuming a number of subsequent impacts with coefficient of restitution e . After the first impact, the impact velocity is reduced by a factor e while the acceleration, \ddot{g}_N , more or less stays the same. The estimated duration till permanent contact is the sum of the infinite sequence of durations given by

$$h_\infty = h_c + eh_c + e^2h_c + \dots = \frac{1}{1-e}h_c. \quad (22)$$

If, at impact, this estimated h_∞ is less than the integration step size h , permanent contact is assumed. The configuration of the system at permanent contact is found by first interpolating the generalized positions and velocities at the time of impact and then doing a fully inelastic impact calculation.

If the two parts are in permanent contact the equations of motion for this constrained mechanical system are according to (8). These together with the contact condition $g_N = 0$ lead to a mixed set of ordinary differential and algebraic equations (DAEs).

$$\begin{bmatrix} \mathbf{M} & \mathbf{g}_N^T \\ \mathbf{g}'_N & \mathbf{0} \end{bmatrix} \begin{bmatrix} \ddot{\mathbf{q}} \\ \lambda_N \end{bmatrix} = \begin{bmatrix} \mathbf{f} \\ -\mathbf{g}''_N \dot{\mathbf{q}}\dot{\mathbf{q}} \end{bmatrix}. \quad (23)$$

These equations can be solved in various ways. In our approach as implemented in the multibody computer code SPACAR [16] the system equations are transformed to a system of independent coordinates. In literature this procedure is often referred to as coordinate partitioning.

4.2.3. Loss of contact

The loss of contact can be detected by monitoring the contact force λ_N . If this force becomes positive, i.e. tension in the contact region, the contact condition, $g_N = 0$, has to be dropped. In finding the zero crossing of the contact force intermediate values can be calculated with the mixed DAEs from (23). For the intermediate values of \mathbf{q} and $\dot{\mathbf{q}}$ the same third-order interpolation polynomial as in (19) can be used. On the other hand, if a numeric integration scheme with intermediate steps is used, like for instance the classic fourth-order Runge–Kutta method, the intermediate values of the contact force can be used for direct interpolation in time. This is a fast and accurate method. In the case of having an intermediate value at the midpoint $h/2$ the second-order interpolation yields

$$\lambda_N(t) = (1 - 3\xi + 2\xi^2)\lambda_{N0} + (4\xi - 4\xi^2)\lambda_{N h/2} + (-\xi + 2\xi^2)\lambda_{N h}, \tag{24}$$

with $\xi = (t - t_n)/h$ and $h = t_{n+1} - t_n$, the contact force λ_{N0} at the beginning, $\lambda_{N h/2}$ at the midpoint, and $\lambda_{N h}$ at the end of the step.

4.2.4. Maximum contact force estimation

The maximum contact force can be estimated from the contact impulse s_N and the elastic material properties of the joint. We shall assume a non-dissipating contact force model according to

$$F_N = K\delta^n. \tag{25}$$

The maximum indentation is calculated from the balance of the kinetic energy just before impact and the elastic energy at maximum indentation,

$$\frac{1}{2}m_e(\dot{\delta}^-)^2 = \frac{1}{n+1}K\delta_{\max}^{n+1}, \tag{26}$$

where m_e is the effective mass (15) of the mechanical system at the contact location. With the contact impulse $s_N = m_e\dot{\delta}^-$ the maximum indentation yields

$$\delta_{\max} = \left(\frac{n+1}{2} \frac{s_N^2}{m_e K} \right)^{1/(n+1)} \tag{27}$$

and the estimated maximum contact force is given by

$$F_{N \max} = \left(\frac{n+1}{2} \frac{K^{1/n}}{m_e} s_N^2 \right)^{n/n+1}. \tag{28}$$

In the case of a Hertzian contact, $n = \frac{3}{2}$ in the above expressions, whereas in the case of a linear spring the exponent n is one and the maximum contact force yields

$$F_{N \max} = \omega_c s_N, \tag{29}$$

where we have introduced the natural contact frequency

$$\omega_c = \sqrt{\frac{K}{m_c}}. \quad (30)$$

In the expression for the contact force (29) we clearly recognize the impact s_N being a product of a high force $F_{N \max}$ and short time period $1/\omega_c$. The approximation for the maximum contact force only holds for high contact frequencies in comparison to the other natural frequencies of the system.

5. Application to a slider-crank mechanism

A slider-crank mechanism is used as an example to illustrate the effect of the different types of joint clearance models. The same mechanism has been used as an example by Ravn [7], which allows us to compare some results. The mechanism, as shown in Fig. 4, consists of a rigid crank of length 0.05 m, a rigid or elastic connecting rod of length 0.12 m and flexural rigidity $EI = 6.2146 \times 10^3 \text{ Nm}^2$, and a slider. The slider mass and the uniformly distributed mass of the connecting rod are both 0.145 kg. The crank rotates at a constant angular velocity $\omega = 523.6 \text{ rad/s}$. The revolute joint between the connecting rod and the slider is modelled with joint clearance. The journal radius is 9.5 mm while the sleeve radius is 10.0 mm. The width of the joint is 20.0 mm. The materials in contact have the properties of steel with Young's modulus $E = 2.06 \times 10^{11} \text{ N/m}^2$, Poisson's ratio $\nu = 0.3$, coefficient of restitution $e = 0.95$ and zero friction is assumed. For the fluid film lubricated journal bearing a lubricant dynamic viscosity of $\mu = 0.1 \text{ N s/m}^2$ is used. In the initial configuration the slider is in the top dead centre and the journal centre displacements and velocities are taken to be zero. Four different cases will be considered. First, all links are considered to be rigid bodies and a Hertzian contact force model is used at the revolute slider joint. Second, again all links are rigid but an impact model at the revolute slider joint is used. Third, a rigid crank and an elastic connecting rod, and a Hertzian contact force model at the revolute slider joint are used. Fourth, all links are assumed to be rigid bodies and a hydrodynamic lubricated bearing at the revolute slider joint is used.

The example is modelled in the general purpose multibody computer code SPACAR [16], which in short can be characterized by finite element method modelling with transformation to independent generalized coordinates. Since clearances are typically at least a 100 times smaller than link lengths the effect of the clearance can be treated as a small perturbation on the ideal kinematic motion. This same treatment is used by Dubowsky and Gardner [17]. The perturbations, being the small displacements in the joint, are handled with the concept of small vibrations superimposed on non-

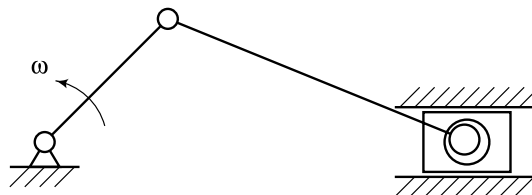


Fig. 4. Slider-crank mechanism with radial clearance at the slider revolute joint.

linear rigid body motion as described by Schwab and Meijaard [18]. This is a fast and accurate method in particular for systems having high eigenfrequencies relative to the driving frequency.

5.1. Continuous Hertzian contact force model

In this first case the links are considered to be rigid bodies and the contact force model for the revolute joint at the slider is of the Hertzian type. This corresponds to the example as given by Ravn [7]. The line contact in the revolute joint will only be present for two cylinders aligned with extreme precision. Also, a uniform force distribution over the length of the joint can only be the case if we neglect the boundary effects. With these arguments we propose to use the Hertzian contact force law between two spheres. With the example parameters from above the Hertzian stiffness coefficient (3) can be calculated with $R_1 = 9.5$ mm and $R_2 = -10.0$ mm as $K = 65.8 \times 10^9$ N/m^{1.5}. The slider accelerations and velocities for the time interval of two crank revolutions, after the transient has died out, are shown in Fig. 5. In the first half of the time interval the accelerations show smooth changes while in the second half they show high peak values which immediately drop back to zero. These zero accelerations indicate the free flight of the slider and consequently the occurrence of impacts in the joint. This is confirmed by step-like changes of the velocity during this second half of the interval. The torque applied to the crank to maintain constant angular velocity is shown in Fig. 6. Here again we observe the high peak values due to the impacts. The rigid slider and crank propagate the high peak forces at the joint instantaneously to the crank. In the path of the journal centre as shown in Fig. 6, we recognize the different contact modes: free flight, impact with rebound, and permanent contact. The dots are plotted equidistantly in time. The excursions outside the clearance circle are due to the local Hertz deformations. Results correspond well with those from Ravn [7].

5.2. Impact model with estimated maximum contact force

In this second case the links are again assumed rigid but the interaction in the revolute joint with clearance is modelled by partly elastic impacts. These impacts give rise to discontinuous

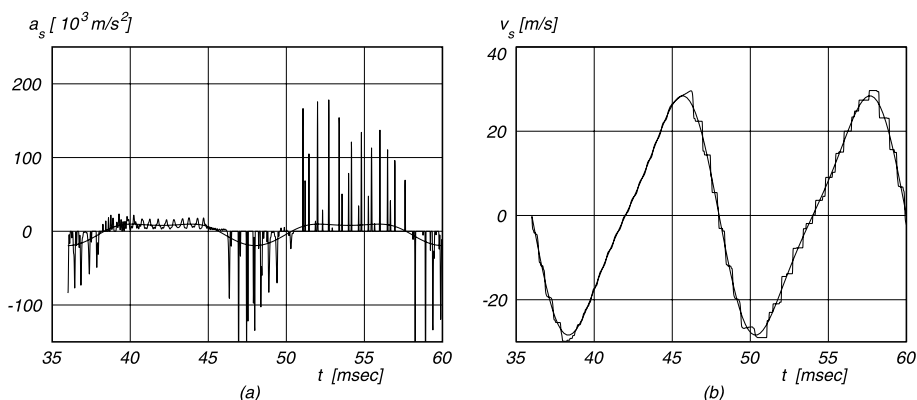


Fig. 5. Acceleration (a) and velocity (b) of the slider for the case of rigid links and a Hertzian contact force model. The smooth curves correspond to the case without clearance. The shown time interval corresponds to two crank revolutions.

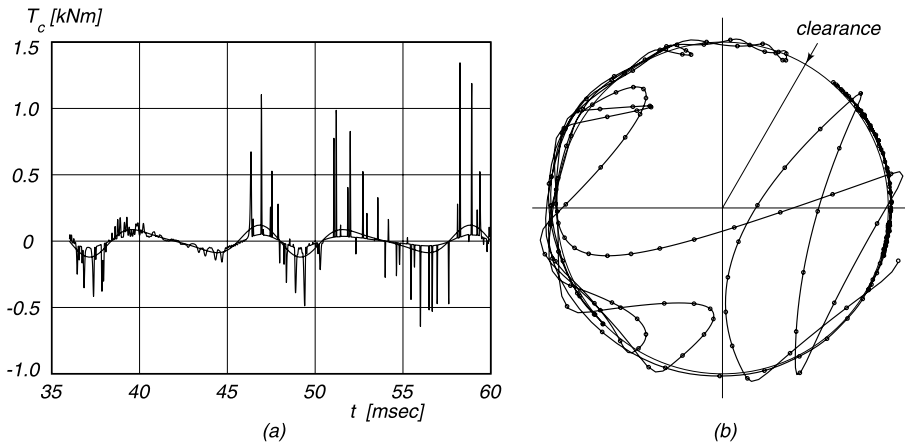


Fig. 6. Torque acting on the crank (a) and journal centre path (b) for the case of rigid links and a Hertzian contact force model. The smooth curve corresponds to the case without clearance. The shown time interval corresponds to two crank revolutions.

forces in the joint and jumps in the velocities of the system. The maximum contact force which occurs during the short period of impact is estimated with the simple model from Section 4.2.4. The slider acceleration and velocity for the time interval of two crank revolutions, after the transient has died out, are shown in Fig. 7. The slider acceleration is zero during most of the first crank revolution. This means that the slider is solely moved by impacts. These impacts can clearly be seen in the staircase-like slider velocity during this first half of the time interval. The second half of the time interval shows permanent contact. The acceleration and velocity oscillate, owing to the tangential oscillation of the journal in the sleeve, around the smooth curve of the rigid solution. In Fig. 8 showing the torques acting on the crank, vertical lines are drawn representing the maximum torques due to the estimated maximum contact forces according to (28). These estimates match well in magnitude and in mutual distance with the high torque peaks during the

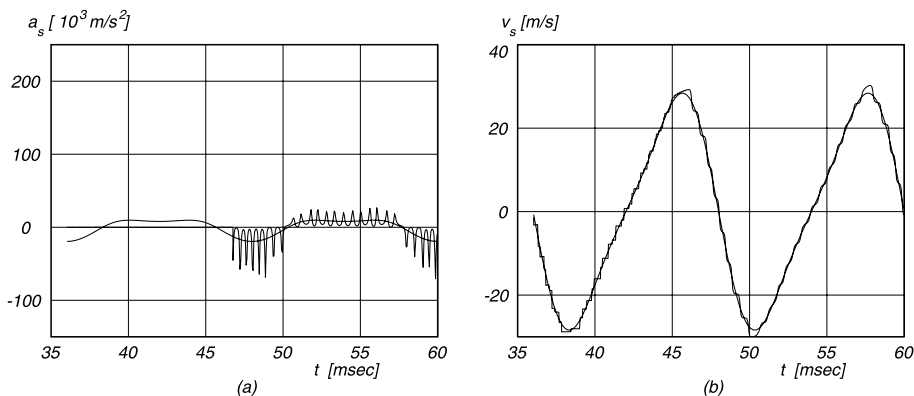


Fig. 7. Acceleration (a) and velocity (b) of the slider for the case of rigid links and an impact contact model. The smooth curves correspond to the case without clearance. The shown time interval corresponds to two crank revolutions.

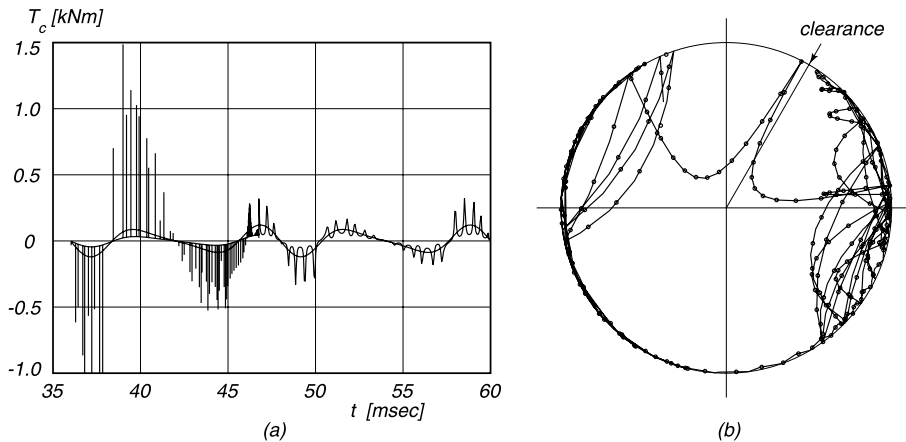


Fig. 8. Torque acting on the crank (a) and journal centre path (b) for the case of rigid links and an impact contact model. In the left figure, the smooth curve corresponds to the case without clearance and the vertical lines indicate the contribution to the torque from the estimated maximum contact force during impact. The shown time interval corresponds to two crank revolutions.

second half of the time interval for the Hertzian contact model from Fig. 6. At the end of the first crank revolution in Fig. 8, a smooth transition from the estimated maximum torque during impact in the permanent contact torque can be observed. In the path of the journal centre we recognize again the different contact modes: free flight, impact with immediate rebound, and permanent contact. The dots are plotted equidistantly in time. Note the zero penetration depths.

5.3. Continuous Hertzian contact force model and elastic connecting rod

In this third case we model the connecting rod as an elastic Euler–Bernoulli beam and the crank as a rigid body, and we use the Hertzian contact force model at the slider joint. The centre line of the connecting rod is assumed inextensible since the frequencies of the axial modes are considerably higher than the frequency of the first bending mode. The material damping in the connecting rod is considered such that the damping of the first eigenmode for small vibrations is 1% of the critical damping. The connecting rod is modelled by two planar beam elements. The model has six degrees of freedom; two degrees of freedom result from the joint clearance and four degrees of freedom describe the bending of the connecting rod. Results are shown in Figs. 9 and 10. The elasticity of the connecting rod has a smoothing effect. Compared with the case where the connecting rod is modelled as a rigid body (Section 5.1), the maximum acceleration is reduced from 180×10^3 to 120×10^3 m/s² and the maximum driving torque from 1.35 to 0.85 kN m. The compliant elements act as a suspension. This effect of elasticity of the links was also noted by Dubowsky and Gardner [17]. During the first crank revolution a high-frequency response in the torque acting on the crank can be observed (see Fig. 10). This is due to high velocity impacts which excite the first and second bending eigenmode of the connecting rod. These eigenfrequencies can be estimated from a simply supported beam model as $\omega_{b1} = 49 \times 10^3$ rad/s and $\omega_{b2} = 197 \times 10^3$ rad/s, and compared with the first eigenfrequency for axial vibrations $\omega_a = 268 \times 10^3$ rad/s

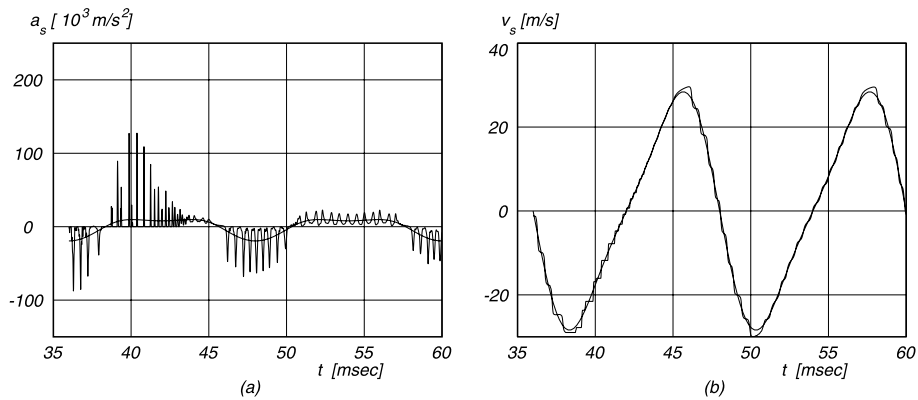


Fig. 9. Acceleration (a) and velocity (b) of the slider for the case of an elastic connecting rod and a Hertzian contact force model. The smooth curves correspond to the case without clearance. The shown time interval corresponds to two crank revolutions.

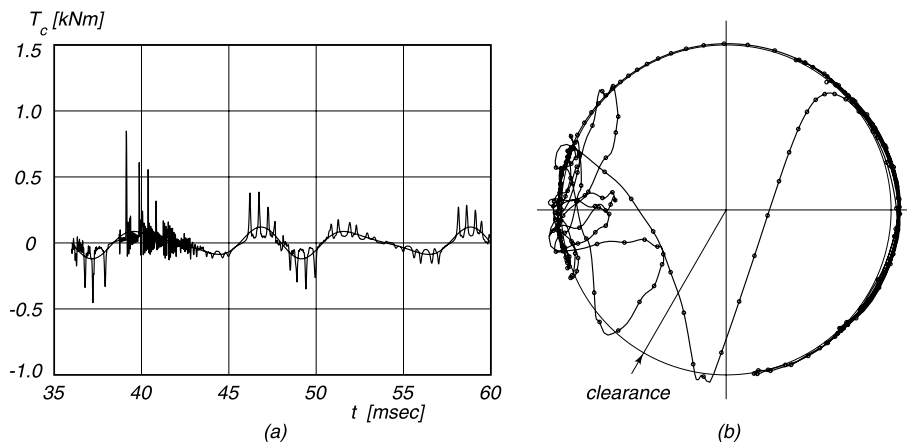


Fig. 10. Torque acting on the crank (a) and journal centre path (b) for the case of an elastic connecting rod and a Hertzian contact force model. The smooth curve corresponds to the case without clearance. The shown time interval corresponds to two crank revolutions.

justify the assumption of the inextensible beam model. The natural contact frequency as in (30) is $\omega_c = 80 \times 10^3$ rad/s, and lies between the first and the second bending eigenfrequency of the rod. The recurring impacts with rebound can also be observed in the journal centre path.

5.4. Continuous contact force model with hydrodynamic lubricated bearing

In this fourth case the links are considered rigid bodies and the revolute slider joint is modelled with a hydrodynamic lubricated fluid film bearing as presented in Appendix A. Looking at the results for this case (Figs. 11 and 12) we see that they are almost the same as for the system without clearance, which are represented by the smoother curves in all figures. The responses

differ only slightly when the slider acceleration has to change sign. The horizontal bearing force F_x has to change sign and the bearing can only supply this by a flight of the journal across the sleeve. This can be seen in the journal centre path diagram (Fig. 12). This crossing will involve high journal centre speeds and subsequently will give rise to peak forces. The velocity of the slider shows clearly that at the extremes it has a tendency to lag behind. Note the steady state behaviour; the first and the second shown crank revolution are practically the same. In the bearing force locus (Fig. 13) the peak force after a change of sign of the horizontal bearing force F_x is evident. The peak force at high velocity and the high stiffness at maximum radial displacement can be observed in Fig. 14 the figure presents a 3D diagram of the magnitude of the bearing force versus the radial displacement and the radial velocity.

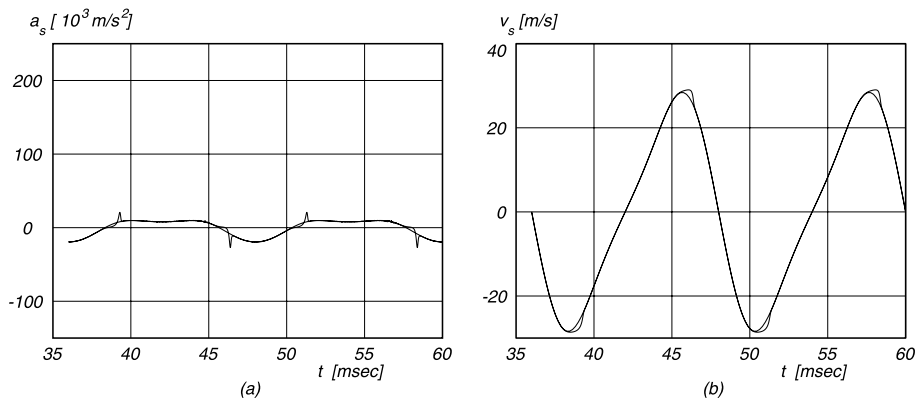


Fig. 11. Acceleration (a) and velocity (b) of the slider for the case of rigid links and a hydrodynamic lubricated bearing model. The smoother curves correspond to the case without clearance. The shown time interval corresponds to two crank revolutions.

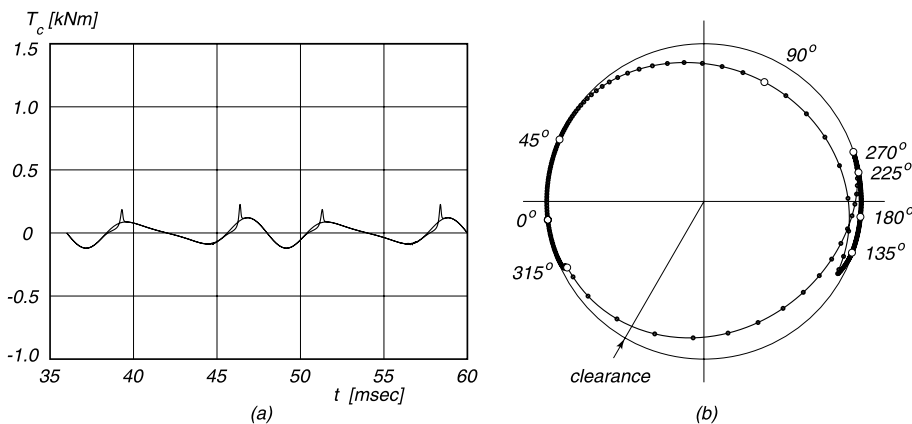


Fig. 12. Torque acting on the crank (a) and journal centre path (b) for the case of rigid links and a hydrodynamic lubricated bearing model. The smooth curve in the left figure corresponds to the case without clearance, the dots with numbers in the right-hand figure indicate the corresponding crank angles. The shown time interval corresponds to two crank revolutions.

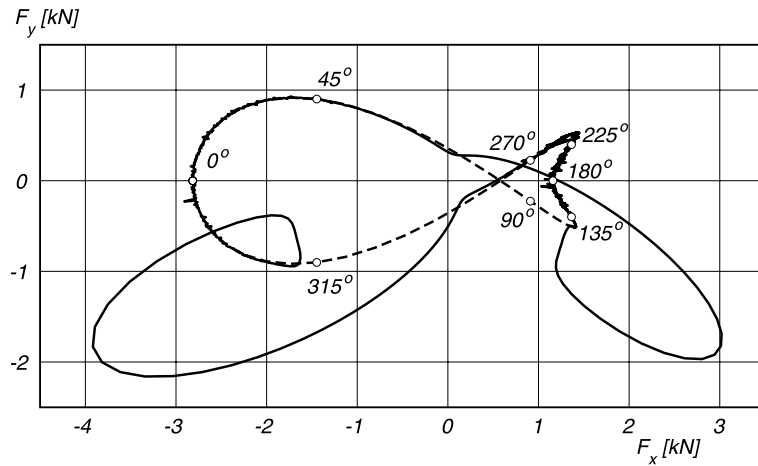


Fig. 13. Bearing force locus for the case of rigid links and a hydrodynamic lubricated bearing model. Dots with numbers indicate the corresponding crank angles. The dashed curve corresponds to the case without clearance.

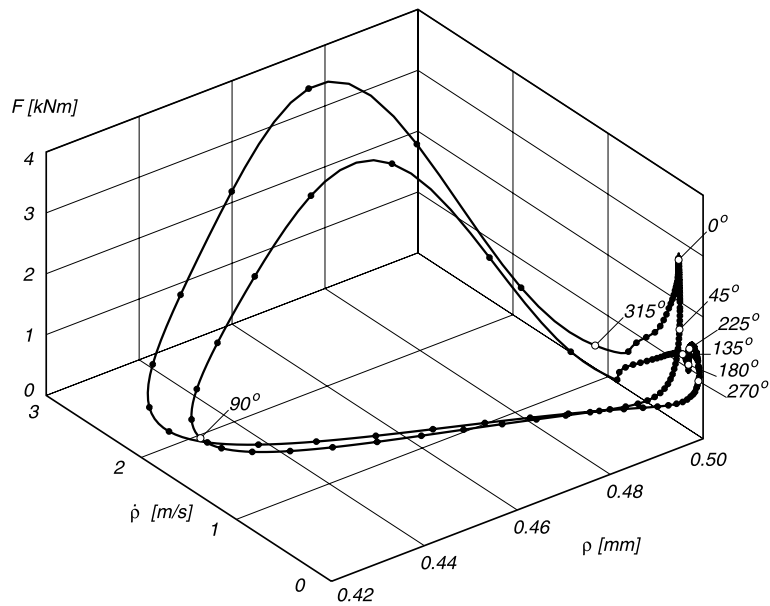


Fig. 14. Magnitude of the bearing force F plotted against the radial displacement ρ and the radial velocity $\dot{\rho}$ for the case of rigid links and a hydrodynamic lubricated bearing model. Dots with numbers indicate the corresponding crank angles.

6. Conclusion

Three clearance models for a revolute joint have been considered: a continuous contact force model, an impact model and a model for a hydrodynamic lubricated bearing. For the impact

model the impulse equations and numerical aspects in handling transitions between different states of motion have been presented; an estimate for the maximal contact force can be made.

The results from the impact model compare well with those from the Hertzian contact force model. Both models can predict the dynamic response of mechanisms and machines having unlubricated revolute joint clearance including the peak values of the forces and position and velocity deviations due to the clearance. The impact model, however, requires much less computational effort.

In the case of a hydrodynamic oil film lubricated bearing the joint forces develop much smoother and the peak values are significantly reduced compared with the unlubricated case. A similar but far smaller reduction can be observed when the links are considered to be elastic. The position and velocity deviations of the system due to the clearance stay approximately the same in both cases. The closed-form analytical expressions for the load bearing properties of a hydrodynamic lubricated fluid film bearing as described by Moes et al. [14] fit well in the numerical procedure. One numerical complication is the high stiffness at large eccentricity.

The examples demonstrate the numerical tool developed to analyse the effect of joint clearances. The software can also be applied to investigate the effect of parameter variations and to optimize revolute joints.

Because of the uncertainty of the unlubricated bearing properties such as the coefficient of restitution and friction, it is recommended that the different models presented in this chapter be tested experimentally. Furthermore, it is recommended that the effect of dry friction be incorporated in the analysis of unlubricated joints in spite of the complexity that this may add to the analysis. For example the friction coefficient will have a significant influence on the tangential oscillations shown in Fig. 7 for the frictionless case.

Appendix A. An algorithm for the fluid film lubricated full journal bearing forces

This appendix gives an algorithmic interpretation of the closed form analytical expressions for the approximate load bearing properties of a fluid film lubricated full journal bearing given by Moes et al. [14]. Their solution is based on the Reynolds equation for a thin film. Incorporated is the finite length of the bearing and the effect of cavitation in the fluid film.

Let us consider a full journal bearing with journal radius r , radial clearance c , bearing length l , and lubricant dynamic viscosity μ . Attached to the sleeve is a Cartesian reference frame Oxy with O in the centre of the sleeve. The position and velocities of the journal centre with respect to the reference frame Oxy of the sleeve are denoted by x , y and \dot{x} , \dot{y} . Let ω be the angular velocity of the journal with respect to the reference frame Oxy , and $\bar{\omega}$ and λ be defined by

$$\begin{aligned}\bar{\omega} &= \omega/2, \\ \lambda &= l/(2r).\end{aligned}\tag{A.1}$$

Then the algorithm is as follows. Calculate the components of the pure-squeeze velocity \mathbf{v} as

$$\begin{bmatrix} v_x \\ v_y \end{bmatrix} = \begin{bmatrix} \dot{x} \\ \dot{y} \end{bmatrix} - \begin{bmatrix} 0 & -\bar{\omega} \\ \bar{\omega} & 0 \end{bmatrix} \begin{bmatrix} x \\ y \end{bmatrix}.\tag{A.2}$$

Let φ be the angle of this vector with the x -axis, and v_s the magnitude,

$$\begin{aligned}\tan \varphi &= v_y/v_x, \\ v_s &= \sqrt{v_x^2 + v_y^2}.\end{aligned}\quad (\text{A.3})$$

Express the scaled journal positions x/c and y/c in the coordinate system rotated over the angle φ ,

$$\begin{bmatrix} \xi \\ \eta \end{bmatrix} = \begin{bmatrix} \cos \varphi & \sin \varphi \\ -\sin \varphi & \cos \varphi \end{bmatrix} \begin{bmatrix} x/c \\ y/c \end{bmatrix}.\quad (\text{A.4})$$

Define the eccentricity as the length of this vector,

$$\varepsilon = \sqrt{\xi^2 + \eta^2}.\quad (\text{A.5})$$

Calculate the dimensionless damping coefficients \mathbf{W}_s or impedance vector for the short bearing (Ocvirk) [19] with ruptured or cavitating fluid film, with

$$\begin{aligned}G_s &= \left(\frac{\lambda}{1 - \varepsilon^2}\right)^2, \\ J_s &= \frac{2}{\sqrt{1 - \varepsilon^2}} \arccos\left(-\frac{\xi}{\sqrt{1 - \eta^2}}\right),\end{aligned}\quad (\text{A.6})$$

as:

$$\begin{aligned}W_{sx} &= G_s((1 - \varepsilon^2 + 3\xi^2)J_s + 6\xi), \\ W_{sy} &= G_s\eta\left(3\xi J_s + 4 + 2\frac{\xi^2}{1 - \eta^2}\right).\end{aligned}\quad (\text{A.7})$$

Calculate the damping coefficients \mathbf{W}_l for the long bearing (Sommerfeld) [19] with ruptured fluid film, with

$$\begin{aligned}G_l &= 3/(2(1 - \varepsilon^2)(1 + \frac{1}{2}\varepsilon^2)), \\ K_l &= \sqrt{(1 + \frac{1}{2}\varepsilon^2)^2 - (1 + \frac{1}{4}\varepsilon^2)\eta^2}, \\ J_l &= \frac{2}{\sqrt{1 - \varepsilon^2}} \arccos\left(-\frac{(1 + \frac{1}{2}\varepsilon^2)\xi}{\sqrt{K_l^2 - \eta^2}}\right),\end{aligned}\quad (\text{A.8})$$

as:

$$\begin{aligned}W_{lx} &= G_l((2 + \varepsilon^2 - 3\eta^2)J_l + 4\xi K_l), \\ W_{ly} &= G_l\eta(3\xi J_l + 4K_l).\end{aligned}\quad (\text{A.9})$$

The damping coefficients of the finite length bearing are approximated by the value as if the short and long bearing damper were connected in series,

$$\begin{aligned}W_x &= 1/(1/W_{sx} + 1/W_{lx}), \\ W_y &= 1/(1/W_{sy} + 1/W_{ly}).\end{aligned}\quad (\text{A.10})$$

The components of the bearing force \mathbf{F} , being the force exerted by the fluid film on the sleeve expressed in the Cartesian reference frame Oxy of the sleeve, are

$$\begin{bmatrix} F_x \\ F_y \end{bmatrix} = 2\mu l \left(\frac{r}{c}\right)^3 v_s \begin{bmatrix} \cos \varphi & -\sin \varphi \\ \sin \varphi & \cos \varphi \end{bmatrix} \begin{bmatrix} W_x \\ W_y \end{bmatrix}. \quad (\text{A.11})$$

References

- [1] R.S. Haines, Survey: 2-dimensional motion and impact at revolute joints, *Mechanism and Machine Theory* 15 (1980) 361–370.
- [2] K. Hain, 'Einflüsse von Gelenkspiel und Reibung auf die im Getriebe wirkenden Kräfte, VDI Fortschrittberichte, Reihe 1: Konstruieren Konstruktionstechnik, nr. 17, VDI Verlag, Düsseldorf, 1969, 105pp.
- [3] K. Soong, B.S. Thompson, A theoretical and experimental investigation of the dynamic response of a slider-crank mechanism with radial clearance in the gudgeon-pin joint, *ASME Journal of Mechanical Design* 112 (1990) 183–189.
- [4] T. Kakizaki, J.F. Deck, S. Dubowsky, Modeling the spatial dynamics of robotic manipulators with flexible links and joint clearances, *ASME Journal of Mechanical Design* 115 (1993) 839–847.
- [5] J.F. Deck, S. Dubowsky, On the limitations of predictions of the dynamic response of machines with clearance connections, *ASME Journal of Mechanical Design* 116 (1994) 833–841.
- [6] L.D. Seneviratne, S.W.E. Earles, Chaotic behaviour exhibited during contact loss in a clearance joint of a four-bar mechanism, *Mechanism and Machine Theory* 27 (1992) 307–321.
- [7] P. Ravn, A continuous analysis method for planar multibody systems with joint clearance, *Multibody System Dynamics* 2 (1998) 1–24.
- [8] H.M. Lankarani, P.E. Nikravesh, A contact force model with hysteresis damping for impact analysis of multibody systems, *ASME Journal of Mechanical Design* 112 (1990) 369–376.
- [9] H.M. Lankarani, P.E. Nikravesh, Continuous contact force models for impact analysis in multibody systems, *Nonlinear Dynamics* 5 (1994) 193–207.
- [10] H. Hertz, Über die Berührung fester elastischer Körper, *Journal für die reine und angewandte Mathematik* 92 (1882) 156–171.
- [11] K.H. Hunt, F.R.E. Crossley, Coefficient of restitution interpreted as damping in vibroimpact, *ASME Journal of Applied Mechanics* 42 (1975) 440–445.
- [12] T.A. Harris, *Rolling Bearing Analysis*, Wiley, New York, 1996.
- [13] R.J. Rogers, G.C. Andrews, Dynamic simulation of planar mechanical systems with lubricated bearing clearances using vector-network methods, *ASME Journal of Engineering for Industry* 99 (1977) 131–137.
- [14] H. Moes, E.G. Sikkes, R. Bosma, Mobility and impedance tensor methods for full and partial-arc journal bearings, *ASME Journal of Tribology* 108 (1986) 612–620.
- [15] J.P. Meijaard, Efficient numerical integration of the equations of motion of non-smooth mechanical systems, *Zeitschrift für angewandte Mathematik und Mechanik* 77 (1997) 419–427.
- [16] J.B. Jonker, J.P. Meijaard, *Spacar*—computer program for dynamic analysis of flexible spatial mechanisms and manipulators, in: W.O. Schiehlen (Ed.), *Multibody Systems Handbook*, Springer-Verlag, Berlin, 1990, pp. 123–143.
- [17] S. Dubowsky, T.N. Gardner, Design and analysis of multilink flexible mechanisms with multiple clearance connections, *ASME Journal of Engineering for Industry* 99 (1977) 88–96.
- [18] A.L. Schwab, J.P. Meijaard, Small vibrations superimposed on a prescribed rigid body motion, *Multibody System Dynamics*, in press.
- [19] O. Pinkus, B. Sternlicht, *Theory of Hydrodynamic Lubrication*, McGraw-Hill, New York, 1961.